Proper motions of Hα filaments in the supernova remnant RCW 86

Helder, E.A.; Vink, J.; Bamba, A.; Bleeker, J.A.M.; Burrows, D.N.; Ghavamian, P.; Yamazaki, R.

DOI
10.1093/mnras/stt993

Publication date
2013

Document Version
Final published version

Published in
Monthly Notices of the Royal Astronomical Society

Monthly Notices
of the
ROYAL ASTRONOMICAL SOCIETY

MNRAS **435,** 910–916 (2013)
Advance Access publication 2013 August 30

doi:10.1093/mnras/stt993

Proper motions of Hα filaments in the supernova remnant RCW 86

E. A. Helder,[1]⋆ J. Vink,[2] A. Bamba,[3] J. A. M. Bleeker,[4] D. N. Burrows,[1]
P. Ghavamian[5] and R. Yamazaki[3]

[1]*The Pennsylvania State University, 525 Davey Lab, University Park, PA 16802, USA*
[2]*Anton Pannekoek Institute/GRAPPA, University of Amsterdam, PO Box 94249, NL-1090 GE Amsterdam, the Netherlands*
[3]*Department of Physics and Mathematics, College of Science and Engineering, Aoyama Gakuin University, 5-10-1 Fuchinobe, Chuo-ku, Sagamihara, Kanagawa 252-5258, Japan*
[4]*SRON Netherlands Institute for Space Research, Sorbonnelaan 2, NL-3584 CA Utrecht, the Netherlands*
[5]*Department of Physics, Astronomy and Geosciences, Towson University, Towson, MD 21252, USA*

Accepted 2013 June 4. Received 2013 May 20; in original form 2012 December 5

ABSTRACT

We present a proper motion study of the eastern shock-region of the supernova remnant RCW 86 (MSH 14-6*3*, G315.4−2.3), based on optical observations carried out with Very Large Telescope/FOcal Reducer and low dispersion Spectrograph 2 in 2007 and 2010. For both the north-eastern and south-eastern regions, we measure an average proper motion of Hα filaments of 0.10 ± 0.02 arcsec yr^{-1}, corresponding to 1200 ± 200 km s^{-1} at 2.5 kpc. There is substantial variation in the derived proper motions, indicating shock velocities ranging from just below 700 km s^{-1} to above 2200 km s^{-1}.

The optical proper motion is lower than the previously measured X-ray proper motion of north-eastern region. The new measurements are consistent with the previously measured proton temperature of 2.3 ± 0.3 keV, assuming no cosmic ray acceleration. However, within the uncertainties, moderately efficient (<27 per cent) shock acceleration is still possible. The combination of optical proper motion and proton temperature rule out the possibility that RCW 86 has a distance less than 1.5 kpc.

The similarity of the proper motions in the north-east and south-east is peculiar, given the different densities and X-ray emission properties of the regions. The north-eastern region has lower densities and the X-ray emission is synchrotron dominated, suggesting that the shock velocities should be higher than in the south-eastern, thermal X-ray dominated, region. A possible solution is that the Hα emitting filaments are biased towards denser regions, with lower shock velocities. Alternatively, in the north-east the shock velocity may have decreased rapidly during the past 200 yr, and the X-ray synchrotron emission is an afterglow from a period when the shock velocity was higher.

Key words: ISM: supernova remnants, cosmic rays.

1 INTRODUCTION

For decades, supernova remnants (SNRs) have been considered the main accelerators of Galactic cosmic rays. One of the earliest arguments for this was their energy budget: in order to maintain the Galactic cosmic ray density, supernovae need to put a substantial amount of their kinetic energy into accelerating cosmic rays. As there are not many sources capable of providing these amounts of energy, there are few other candidates (for a list, see Butt 2009). The idea that SNRs are the main sources of cosmic rays has been thoroughly investigated, both from the theoretical and observational perspective (Helder et al. 2012; Schure et al. 2012, for recent reviews).

One method of testing whether SNRs are efficiently accelerating cosmic rays is by investigating the energy budget from the hot plasma in the remnants. This method compares the energy in thermal particles right behind the shock front to the total kinetic energy available (deduced from the shock speed). If the available kinetic energy is not fully used for heating particles, one can attribute the energy deficit to energy in *non*-thermal particles (e.g., Vink et al. 2010). This method has been used to determine the cosmic ray pressure behind the shock fronts of four remnants: 1E 0102−7219, the Cygnus Loop, SNR 0509−67.5 and RCW 86 (Hughes, Rakowski & Decourchelle 2000; Helder et al. 2009; Salvesen, Raymond & Edgar 2009; Helder, Kosenko & Vink 2010, respectively). For the first two remnants, the temperatures are based on the electron temperature measured from X-ray spectra. This method has the additional difficulty that the electron temperature does not necessarily provide

⋆E-mail: helder@psu.edu

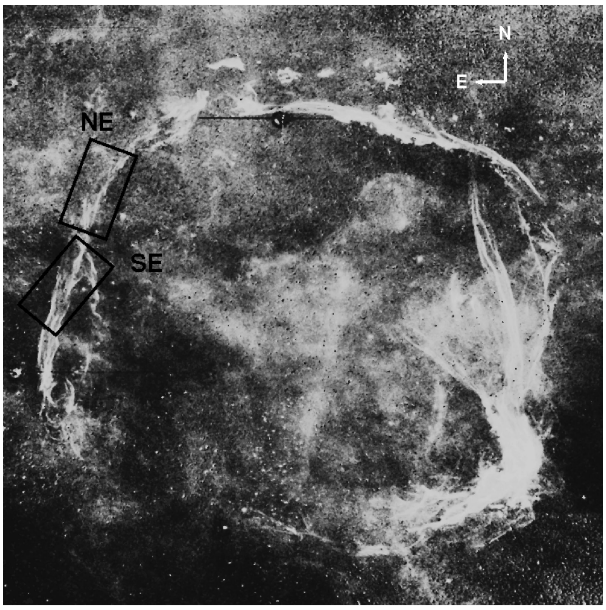

Figure 1. Hα image of the RCW 86 SNR (Smith 1997). Indicated are the locations of the pointings for which we determined proper motions in the north-east (NE) and south-east (SE), shown in Fig. 2.

an adequate measure of the mean post-shock plasma temperature (Ghavamian, Laming & Rakowski 2007).

The temperatures in the studies by Helder et al. (2009, 2010) are based on the post-shock proton temperature. For solar abundances, the proton temperature is more than half the mean plasma temperature. The proton temperatures in these studies were measured from the Hα line emission. For non-radiative shocks in partially neutral gas, this Hα line emission consists of both a narrow and a broad component superimposed. The narrow component is caused by direct excitation of the neutral hydrogen after being swept up by the shock. The broad component is emitted after charge exchange between the swept-up neutral hydrogen atoms and the hot post-shock protons. The width of this component is therefore a measure of the post-shock proton temperature (see Heng 2010, for a review).

A disadvantage of the shock velocity measurements for north-eastern part of RCW 86 by Helder et al. (2009) is that they are based on X-ray proper motion measurements. Because of the limited statistics of the X-ray images the proper motions were measured for large regions. In contrast, the temperature measurements based on Hα spectroscopy are measured at very specific locations that are relatively bright in Hα. It is, therefore, preferable to combine Hα-based temperature measurements with proper motions of specific Hα filaments. For that reason, we obtained new Hα images of the north-eastern and south-eastern parts of RCW 86 (MSH 14-6*3*, G315.4−2.3, see Fig. 1) in order to measure the proper motions for those specific regions for which we had also measured the proton temperatures. We present those results here.

2 DATA AND RESULTS

The two epochs of data for this study were obtained with Very Large Telescope (VLT)/FOcal Reducer and low dispersion Spectrograph 2 (FORS2) (Appenzeller et al. 1998). The first observation was done on 2007 February 25 and the second observation on 2010 April 5. This gives a time baseline of 1135 d. For this study, we focus on the observations centred on the north-east (RA: $14^{\rm h}45^{\rm m}11^{\rm s}$, Dec.: $-62^\circ17'43''$, J2000) and south-east (RA: $14^{\rm h}45^{\rm m}30^{\rm s}$, Dec.: $-62^\circ25'21''$, J2000) of the remnant. Both observations include three images through an Hα filter (`H_Alpha+83`) for 10 min in total per epoch as well as three images through an Hα filter with a velocity offset of 4500 km s^{-1} (`H_Alpha/4500+61`), also for a total of 10 min per pointing per epoch. The three frames were spatially dithered to account for potential small-scale imperfections in the detector. The biases were subtracted, and to correct for the uneven illumination across the detector, we used sky flats. Then the frames were combined for each epoch and filter. The individual images were aligned using the `interpol` routine of the image subtraction package ISIS (Alard & Lupton 1998). In this routine a two-dimensional linear function is fitted to the positions of more than 350 stars per frame (exact number differs per frame) and the frames are remapped to match the corresponding stars in the reference frame. To subtract stars and other non-Hα background emission, we subtracted images through the `H_Alpha/4500+61` continuum filter from the images through the Hα filter. The continuum images were scaled such that the resulting subtracted image would have the lowest standard deviation, bringing the subtracted sky emission down to zero. The resulting images are shown in Fig. 2. We determined the scale of the images to be 0.252 arcsec pixel^{-1} by matching the images with the USNO-B1.0 catalogue (Monet et al. 2003) from which we picked isolated stars. We utilized the same stars to estimate the spatial accuracy of our image matching. We determined the pixel coordinates of the centroids of these stars in both images. These coordinates all matched within 0.25 pixels for the north-east, and 0.12 pixels for the south-east. We conservatively consider these offsets to be the systematical error on our proper motion measurements.

We made a mask for each image, to flag pixels that contain either cosmic ray streaks or stars. We used a median filter for detecting cosmic rays and faint stars, and we set a maximum luminosity to detect bright stars.

Since RCW 86 is located in the Galactic plane, the field is crowded with background stars. To measure the proper motions as accurately as possible, we avoided filaments with stars in their close vicinity. Keeping this in mind, we selected regions across several filaments. We also made sure to cover the filaments that were used for the spectra described in Helder et al. (2009) and Helder et al. (2011, regions 1 and 3 for the south-east and regions 6, 7 and 8 for the north-east, Fig. 2). We extracted surface brightness profiles from these filaments. To correct for intrinsic brightness variations of the background of the images, we determined and subtracted the background in both the 2007 and 2010 profiles independently.

To calculate the proper motions, we shifted the profiles over one another in steps of 1 pixel, calculating the χ^2 for each shift, assuming a constant error for all bins (Fig. 3). We determine the best-fitting shift by fitting a parabola to the seven χ^2 values surrounding the minimal χ^2. The surface brightness uncertainties were estimated, iteratively, from the dispersion of the residuals around the best-fitting model. This results per definition in $\chi^2_{\rm red} = 1$. Utilizing these surface-brightness uncertainty estimates, we estimate the 1σ uncertainties on the best-fitted proper motion, which correspond to $\Delta\chi^2 = 1$. Tables 1 and 2 list the proper motions and 1σ uncertainties resulting from this procedure.

3 DISCUSSION

The Hα proper motion measurements for the eastern region of RCW 86 reported in our study provide some interesting results. First, the proper motions in the north-east do not agree with the X-ray proper motion of the X-ray synchrotron region. The X-ray proper motion

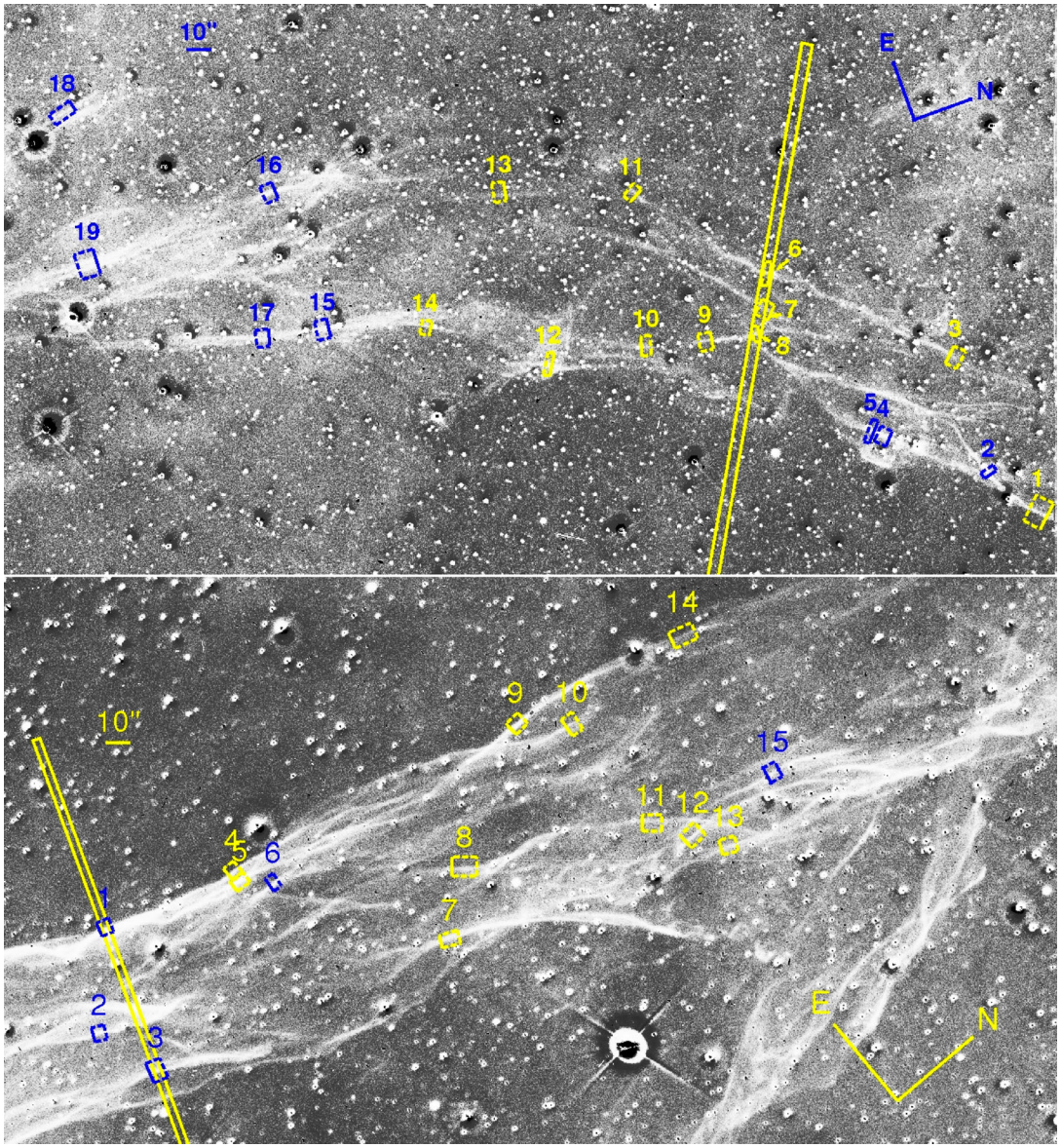

Figure 2. VLT/FORS2 images of the north-east (top) and south-east (bottom) part of the remnant. Both observations were obtained in 2010 and both images have been continuum subtracted. North and east are indicated, as well as the scale and the regions we choose for determining proper motions (marked by the small boxes). The long rectangular boxes indicate the locations of the slits used in Helder et al. (2009) and Helder, Vink & Bassa (2011). For the top image, the centre of the remnant is below, for the bottom image, it is below and slightly to the right. The colours of the boxes were chosen to aid visibility in both lighter and darker parts of the image.

reported by Helder et al. (2009) is 0.5 ± 0.2 arcsec yr^{-1}, whereas for the north-east the error-weighted average of all measured optical proper motions is 0.095 ± 0.03 arcsec yr^{-1}. This is a 2σ deviation from the X-ray proper motion.

Secondly, we do not find a substantial difference in optical proper motion between the north-eastern, X-ray synchrotron-emitting, part of the remnant shell and the south-eastern shell, whose X-ray emission only shows evidence for thermal X-ray emission (e.g. Vink et al. 2006). For the south-east the error-weighted average proper motion is 0.10 ± 0.02 arcsec yr^{-1}.

3.1 Implications for shock acceleration efficiency

Both findings have implications for the particle acceleration properties of RCW 86. For a nominal distance of RCW 86 of 2.5 kpc, a proper motion of 0.10 arcsec yr^{-1} corresponds to a shock velocity of 1180 km s^{-1}. A shock with this velocity is expected to heat the protons to at least $kT_{\rm expected} = (3/16)\mu m_{\rm p} V_{\rm s}^2 = 1.6$ keV, with $\mu = 0.6$ in case of full electron–ion equilibration and $\mu = 1$ if protons and electrons are completely unequilibrated (i.e. the temperature is proportional to the particle mass, and all species have equal velocity distribution instead of equal energy distributions). This is consistent with the proton temperature of $kT_{\rm p} = 2.3 \pm 0.3$ keV based on the width of the broad Hα line reported by Helder et al. (2009), as illustrated in Fig. 4. Note that for the south-eastern part Helder et al. (2011) published two temperature measurements. For the north-eastern part only one temperature was published.

Since there is no longer a discrepancy between the temperature expected from the proper motion and the measured proton temperature, there is also no need to infer that a significant

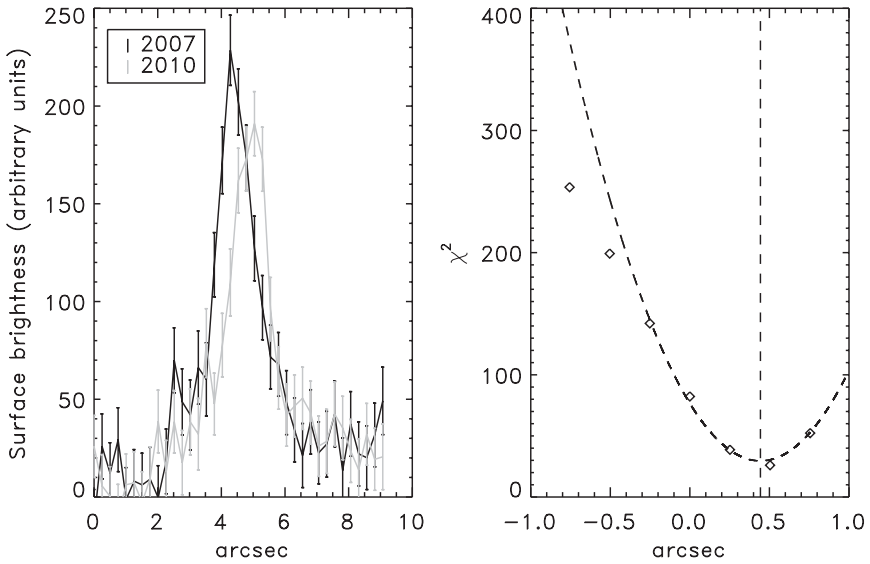

Figure 3. Left: surface brightness profiles taken in 2007 and 2010 of region 6 in the north-east part of the remnant. Right: χ^2 values as function of filament displacement. The dashed line indicates the best-fitting displacement.

Table 1. Proper motions for the north-east pointings. Quoted uncertainties are the statistical 1σ uncertainties. Systematic uncertainties are 0.063 arcsec and 240 km s^{-1}. The last row contains the average values and standard deviation.

Filament #	Shift (arcsec) in 1135 d	V_s (km s^{-1})	@ ±	2.5 kpc Stat. err.
1	0.20 ± 0.04	745	±	136
2	0.14 ± 0.07	543	±	280
3	0.31 ± 0.09	1172	±	347
4	0.25 ± 0.05	948	±	174
5	0.28 ± 0.05	1067	±	186
6	0.49 ± 0.07	1871	±	250
7	0.31 ± 0.10	1196	±	367
8	0.35 ± 0.06	1325	±	221
9	0.34 ± 0.05	1299	±	191
10	0.08 ± 0.11	317	±	437
11	0.31 ± 0.09	1192	±	351
12	0.26 ± 0.04	991	±	133
13	0.39 ± 0.12	1493	±	475
14	0.21 ± 0.10	800	±	371
15	0.26 ± 0.07	1001	±	256
16	0.37 ± 0.05	1422	±	175
17	0.29 ± 0.06	1096	±	219
18	0.81 ± 0.23	3071	±	878
19	0.35 ± 0.04	1349	±	151
Mean/std. dev.	0.31/0.08	1204	/	575

Table 2. Proper motions for the south-east pointings. Quoted uncertainties are the statistical 1σ uncertainties. Systematic uncertainties are 0.03 arcsec and 114 km s^{-1}

Filament #	Shift (arcsec) in 1135 d	V_s (km s^{-1})	@ ±	2.5 kpc Stat. err.
1	0.40 ± 0.04	1531	±	144
2	0.13 ± 0.04	478	±	137
3	0.28 ± 0.06	1082	±	225
4	0.38 ± 0.05	1446	±	179
5	0.22 ± 0.03	852	±	121
6	0.35 ± 0.05	1330	±	175
7	0.43 ± 0.06	1653	±	228
8	0.38 ± 0.04	1431	±	137
9	0.38 ± 0.04	1444	±	158
10	0.37 ± 0.07	1403	±	256
11	0.24 ± 0.13	910	±	501
12	0.18 ± 0.12	671	±	448
13	0.33 ± 0.06	1246	±	230
14	0.49 ± 0.07	1881	±	248
15	0.32 ± 0.08	1213	±	289
Mean/std. dev	0.33/0.10	1240	/	374

fraction of the shock's energy flux has been lost to cosmic ray acceleration.

However, there is sufficient uncertainty in the distance and proper motion to allow still for the possibility of (moderately) efficient shock acceleration: at the slit position for which the proton temperature was measured (filaments 6, 7, 8) the proper motion is 0.13 ± 0.02 arcsec yr^{-1} (error-weighted average, including systematic errors). If the distance to RCW 86 is at the high-end of the estimates, 3 kpc, this corresponds to 1792 ± 258 km s^{-1}. This translates into an upper limit on the ratio between measured and expected post-shock temperature of $\beta \equiv kT_p/kT_{expected} > 0.61$, corresponding to a limit on the post-shock cosmic ray pressure of $w \equiv P_{cr}/P_{tot} < 27$ per cent, according to the two-fluid model of Vink et al. (2010). The 2σ error on the reported proper motion allows in principle even for an upper limit on the shock velocity of <2300 km s^{-1}, corresponding to $kT_p < 6.2$ keV, $\beta > 0.37$ and an efficiency of $w < 46$ per cent.

On the other hand the combination of measured proton temperature (Helder et al. 2009) and the proper motions reported here reinforces the distance estimates of 2.5 ± 0.5 kpc (Rosado et al. 1996; Sollerman et al. 2003), and make a distance between 1.0 and 1.5 kpc (Long & Blair 1990; Bocchino et al. 2000) less likely, since for the measured proton temperature of 2.3 ± 0.3 keV, a shock velocity is required of at least 1080±70 km s^{-1}. This is at odds with our proper motion measurements, which for 1.0–1.5 kpc imply shock velocities of only 400–700 km s^{-1}.

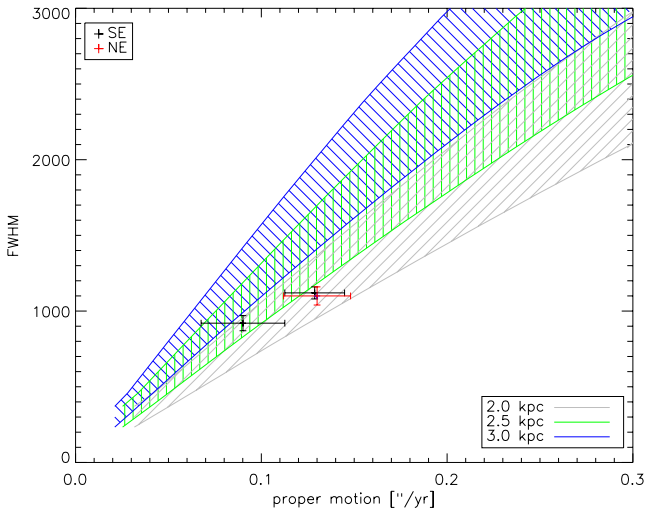

Figure 4. Proper motion measurements of the south-east (black) and north-east (red) filaments combined with the measurements of Helder et al. (2009) of the FWHM of the broad components for these filaments. Overplotted are the line widths (FWHM) as function of velocity for a range of distances (van Adelsberg et al. 2008).

3.2 Implications for the X-ray synchrotron emission

Although the efficient cosmic ray acceleration in the north-east of RCW 86 is no longer necessary to explain the observations, the Hα proper motions pose some new challenges for understanding the properties of this SNR.

First, the X-ray emission properties of the north-eastern and south-eastern filaments are quite distinct. The north-east is dominated by X-ray synchrotron emission with only weak X-ray line emission from part of the region. The weak line emission indicates a low-ionization age, implying a combination of low-density and/or recently heated plasma. In contrast, the south-east filaments do not show any signs of X-ray synchrotron radiation, but have much brighter thermal X-ray emission than the north-east, indicating higher plasma densities and also larger ionization ages (Vink et al. 2006). The Hα emission in the north-east is also fainter than in the south-east, consistent with the idea that in the north-east the shock moves through a lower density medium than in the south-east. Given the apparent contrast in densities, one also expects distinct shock velocities, as the shock is expected to slow down in denser regions. This is inconsistent with the low and similar Hα proper motions measured for the north-east and south-east.

The presence of X-ray synchrotron emission in the north-east is consistent with relatively high shock velocities. This was the reason for investigating the shock acceleration properties of the northeast shock by Helder et al. (2009). Diffusive shock acceleration models show that for synchrotron radiation with maximum photon energy limited by radiative losses, the cut-off photon energy is independent of magnetic field and scales as (Zirakashvili & Aharonian 2007; Vink 2012)

$$h\nu_{\rm cut-off} \approx 1.4\eta^{-1}\left(\frac{V_{\rm s}}{5000\ {\rm km\ s^{-1}}}\right)^2\ {\rm keV}, \quad (1)$$

with η ($\geq$1) an efficiency factor with respect to optimal Bohm-diffusion (e.g. Reynolds 1998). Indeed most SNR shocks for which X-ray synchrotron radiation has been detected appear to have shock velocities in excess of 3000 km s^{-1} (Helder et al. 2012). Clearly the Hα proper motions reported here do not agree with this general trend, as for a distance of 2.5 kpc the proper motions should correspond to $h\nu_{\rm cut-off} < 0.1$ keV. This low value is consistent with the lack of X-ray synchrotron radiation in the south-east, but is at odds with the prominence of X-ray synchrotron radiation from the north-east. Note that also the High Energy Stereoscopic System TeV γ-ray map of RCW 86 indicates a lack of TeV emission from the south-east (Aharonian et al. 2009).

Here, we offer two possible explanations for the presence of the X-ray synchrotron radiation from the north-eastern region and its absence from the south-eastern region.

First, it is possible that the overall shock velocity in the north-east is not well represented by the Hα proper motions, as suggested by Williams et al. (2011). Note that it is not uncommon for supernova shock speed measurements at different wavelengths to give contradictory answers in different wavelengths (Moffett, Goss & Reynolds 1993). RCW 86 is characterized by large density contrasts, so perhaps we only detect Hα emission where locally the shock encounters denser gas, and (temporarily) slows down, thereby increasing in Hα brightness. In this context it is interesting to note that all along the south-eastern shock Hα emission is present, whereas the north-eastern shock region does not show evidence for Hα everywhere along the shock region. The strong variation in densities could in principle mean that the overall shock velocity in the north-east is closer to 3000 km s^{-1}, consistent with the X-ray proper motions reported by Helder et al. (2009), but that the Hα emitting regions are much slower. Indeed, the measured proper motions show variation that cannot be explained by statistical measurement errors. For example, filament 18 has a proper motion that is 2σ higher than the average proper motion, and indicates that locally the shock velocity may be higher than 2000 km s^{-1}. In contrast, filament 1 corresponds to a 2.5σ deviation on the low side $V_{\rm s} \approx$ 750km s^{-1}. The problem of explaining the X-ray/optical proper motion discrepancy in the north-east with large variations in shock velocities is that shocks in the south-east also show significant variation in proper motion. In order to test this explanation it is important to obtain another X-ray proper motion measurement, now with a longer baseline and therefore reduced measurement error.

The second, alternative, explanation is that the Hα proper motions reported here are representative of the overall shock velocity in both the north-eastern and south-eastern regions, but that in the north-east the shock velocity was much higher in the recent past. Vink et al. (2006) reported for this region a magnetic field of $B \approx 26\ \mu$G, consistent with the interpretation of GeV and TeV γ-ray observations of RCW 86 (Aharonian et al. 2009; Lemoine-Goumard et al. 2012). For these magnetic fields, a relativistic electron with an energy of $\sim$100 TeV has a synchrotron loss time of $\sim$180 yr. Therefore, it is possible that 200 yr ago, the shock velocity was higher than 3000 km s^{-1} and nowadays, the region is still glowing in X-ray synchrotron radiation. This does not necessarily imply that there was a problem with the X-ray proper motion, as the X-ray proper motion measures the velocity of the downstream plasma of the whole X-ray shell in the north-east, rather than the shock velocity. Although a long X-ray synchrotron loss time in combination with a low shock velocity offers an explanation for the X-ray synchrotron emission from the north-east, it does not offer an explanation for the absence of X-ray synchrotron radiation from the south-east. Given the higher density in the south-east the deceleration of the shock in the south-east should have been more severe, whereas the Hα proper motions for the two regions are comparable.

To complicate matters, one could also invoke magnetic field orientation as an additional ingredient for the presence or absence of X-ray synchrotron radiation. For example, the geometry of the X-ray synchrotron emission from SN 1006 suggests that in this

SNR X-ray synchrotron emission only occurs when the magnetic field is parallel to the shock normal (Rothenflug et al. 2004). In RCW 86 the X-ray synchrotron emitting regions are roughly south-west–north-east aligned, more or less parallel to the Galactic plane. However, the morphology is not as clear as for SN 1006, and it does not agree with the idea that in the south-west the X-ray synchrotron emission is associated with the reverse shock, rather than with the forward shock (Rho et al. 2002).

A possible explanation for the different X-ray properties of the south-eastern and north-eastern regions could be offered by the hydrodynamic simulations of SNRs evolving in a wind-blown cavity (Dwarkadas 2005). RCW 86 is regarded to be such an SNR (Vink, Kaastra & Bleeker 1997; Vink et al. 2006; Williams et al. 2011). The simulations indicate that the shock velocity rapidly decreases once it starts interacting with the shell surrounding the cavity, but it recovers some of the shock velocity once it has penetrated the shell. The reason is that the initial interaction of the shock wave with the shell results in a slowing down of the shock, but as more of the material behind the shock transfers energy and momentum to the shell, it speeds up again. In the simulation presented by Dwarkadas (2005, case 2) the shell is encountered around 4000 yr, and as a result the shock velocity drops from $\sim$3000 km s^{-1}, to a few hundred km s^{-1}, but within a few hundred years the shock regains speed and continues with $\sim$1000 km s^{-1}. These numbers are for the specific case simulated, but it is conceivable that in different regions of RCW 86 the SNR shock is in different stages of interacting with the shell. In the north-east the shock could be approaching or just hitting the shell, and could therefore be rapidly decelerating. In the south-east this could have happened in the more distant past, and the shock may actually have picked up speed again. In such a situation one can still expect X-ray synchrotron radiation in the north-east, but in south-east the shock slowed down too long ago to still have electrons present with energies in excess of 10 TeV.

This interpretation is not entirely satisfying, as one would expect somewhere on the eastern side to find a region that is in the stage of the interaction with the shell with the slowest shock velocities. Inspecting the variation in velocity over the filaments there is not an obvious south-north trend. Instead, we find that in the north-east the inner filaments (north-east 1, 2, 4, 10, 12, 14) to have the lowest velocities.

4 CONCLUSIONS

We measured proper motions of the Hα emitting shock fronts on the east side of the RCW 86 SNR. Based on our study, we reach the following conclusions.

(i) The shock velocities in the eastern part of the remnant display a large spread, varying from $>$700 km s^{-1} to above 2200 km s^{-1} assuming a distance of 2.5 kpc.

(ii) These shock velocities are consistent with what we would expect from the proton temperatures determined from the broad Hα lines in the south-east and north-east by Helder et al. (2009, 2011); Ghavamian et al. (2001) and Ghavamian et al. (2007).

(iii) Assuming a distance of 2.5 kpc, we do not need any cosmic ray pressure to explain the proton temperature in the north-east of RCW 86.

(iv) Taking into account measurement and distance uncertainties, a moderately efficient shock acceleration is still possible, with $<$27 per cent of the post-shock pressure being provided by accelerated particles.

(v) The combination of the proper motion and the post-shock proton temperature rules out a distance of less than 1.5 kpc for this remnant.

(vi) The proper motions of the filaments in the south-east and north-east are similar, which is surprising, given the very different nature of the dominant X-ray emission mechanism of these regions, namely synchrotron in the north-east and thermal X-ray emission in the south-east. We discuss two possible explanations for this. The first is that the Hα emitting parts of the shocks have slowed down, whereas the X-ray synchrotron emitting shocks are still moving fast through the ambient medium, as suggested by Williams et al. (2011). The second explanation is that the X-ray expansion measurement was inaccurate, and the entire north-east shock has slowed down recently by interaction with a dense shell, and is still glowing in X-ray synchrotron radiation. The south-east shock has also slowed down by the same shell but has already overcome this shell and the shock velocity has increased again. The two scenarios can be distinguished by obtaining a more accurate X-ray proper motion measurement with a new *Chandra* observation, providing a much longer baseline.

ACKNOWLEDGEMENTS

EAH expresses her gratitude to Ana Chies Santos and Angela Adamo for discussions on the reduction of optical data. EAH and DNB are supported by SAO grants GO1-12070X and GO2-13064X. This research is based on observations collected with ESO telescopes at the Paranal Observatory under programme IDs 079. D-0735(A) and 385.D-0483(A).

REFERENCES

Aharonian F. et al., 2009, ApJ, 692, 1500
Alard C., Lupton R. H., 1998, ApJ, 503, 325
Appenzeller I. et al., 1998, The Messenger, 94, 1
Bocchino F., Vink J., Favata F., Maggio A., Sciortino S., 2000, A&A, 360, 671
Butt Y., 2009, Nat, 460, 701
Dwarkadas V. V., 2005, ApJ, 630, 892
Ghavamian P., Raymond J., Smith R. C., Hartigan P., 2001, ApJ, 547, 995
Ghavamian P., Laming J. M., Rakowski C. E., 2007, ApJ, 654, L69
Helder E. A., Kosenko D., Vink J., 2010, ApJ, 719, L140
Helder E. A., Vink J., Bassa C. G., 2011, ApJ, 737, 85
Helder E. A. et al., 2009, Sci, 325, 719
Helder E. A., Vink J., Bykov A. M., Ohira Y., Raymond J. C., Terrier R., 2012, Space Sci. Rev., 173, 369
Heng K., 2010, PASA, 27, 23
Hughes J. P., Rakowski C. E., Decourchelle A., 2000, ApJ, 543, L61
Lemoine-Goumard M., Renaud M., Vink J., Allen G. E., Bamba A., Giordano F., Uchiyama Y., 2012, A&A, 545, A28
Long K. S., Blair W. P., 1990, ApJ, 358, L13
Moffett D. A., Goss W. M., Reynolds S. P., 1993, AJ, 106, 1566
Monet D. G. et al., 2003, AJ, 125, 984
Reynolds S. P., 1998, ApJ, 493, 375
Rho J., Dyer K. K., Borkowski K. J., Reynolds S. P., 2002, ApJ, 581, 1116
Rosado M., Ambrocio-Cruz P., Le Coarer E., Marcelin M., 1996, A&A, 315, 243
Rothenflug R., Ballet J., Dubner G., Giacani E., Decourchelle A., Ferrando P., 2004, A&A, 425, 121
Salvesen G., Raymond J. C., Edgar R. J., 2009, ApJ, 702, 327
Schure K. M., Bell A. R., O'C Drury L., Bykov A. M., 2012, Space Sci. Rev., 173, 491
Smith R. C., 1997, AJ, 114, 2664
Sollerman J., Ghavamian P., Lundqvist P., Smith R. C., 2003, A&A, 407, 249

van Adelsberg M., Heng K., McCray R., Raymond J. C., 2008, ApJ, 689, 1089
Vink J., 2012, A&AR, 20, 49
Vink J., Kaastra J. S., Bleeker J. A. M., 1997, A&A, 328, 628
Vink J., Bleeker J., van der Heyden K., Bykov A., Bamba A., Yamazaki R., 2006, ApJ, 648, L33
Vink J., Yamazaki R., Helder E. A., Schure K. M., 2010, ApJ, 722, 1727
Williams B. J. et al., 2011, ApJ, 741, 96
Zirakashvili V. N., Aharonian F., 2007, A&A, 465, 695

This paper has been typeset from a TEX/LATEX file prepared by the author.